

Free-standing hydrogel-particle composite membrane with dynamically controlled permeability

Khulan Sergelen, Christian Petri, Ulrich Jonas, and Jakub Dostalek

Citation: *Biointerphases* **12**, 051002 (2017);

View online: <https://doi.org/10.1116/1.4996952>

View Table of Contents: <http://avs.scitation.org/toc/bip/12/5>

Published by the [American Vacuum Society](#)

Spectra
Simplified

Plot, compare, and validate
your data with just a click

eSpectra:
surface science

SEE HOW IT WORKS



Free-standing hydrogel-particle composite membrane with dynamically controlled permeability

Khulan Sergelen

BioSensor Technologies, AIT-Austrian Institute of Technology GmbH, Muthgasse 11, 1190 Vienna, Austria
and Center for Biomimetic Sensor Science, Nanyang Technological University, 50 Nanyang Avenue, 637553
Singapore

Christian Petri and Ulrich Jonas

Macromolecular Chemistry, University of Siegen, Adolf-Reichwein-Strasse 2, 57076 Siegen, Germany

Jakub Dostalek^{a)}

BioSensor Technologies, AIT-Austrian Institute of Technology GmbH, Muthgasse 11, 1190 Vienna, Austria

(Received 20 July 2017; accepted 14 November 2017; published 6 December 2017)

The preparation and investigation of a free-standing membrane made from a composite of thermoresponsive poly(*N*-isopropylacrylamide) (pNIPAAm) and polystyrene nanoparticles (PS NP) with temperature-controlled permeability is reported. The method exploits the light-induced crosslinking of the photo-reactive pNIPAAm-based polymer and mechanical reinforcement of the membrane structure by the polystyrene nanoparticles. About micrometer thick layers were either directly attached to a gold surface or prepared as free-standing layers spanning over arrays of microfluidic channels with a width of about hundred microns by using template stripping. Diffusion of liquid medium, low molecular weight molecules, and large molecular weight proteins contained in blood through the composite membrane was observed with combined surface plasmon resonance (SPR) and optical waveguide spectroscopy (OWS). The swelling ratio, permeability, and nonspecific sorption to these composite membranes were investigated by SPR and OWS as a function of molecular weight of analyte, loading of PS NP in the composite film, and temperature. The authors show successful preparation of a defect-free membrane structure that acts as a thermoresponsive filter with nanoscale pores spanning over an area of several square millimeters. This membrane can be reversibly switched to block or allow the diffusion of low mass molecules to the sensor surface by temperature-triggered swelling and collapsing of the hydrogel component. Blocking of diffusion and low unspecific sorption of proteins contained in blood serum is observed. These features make this platform interesting for potential future applications in continuous monitoring biosensors for the analysis of low molecular weight drug analytes or for advanced cell-on-chip microfluidic studies.

© 2017 Author(s). All article content, except where otherwise noted, is licensed under a Creative Commons Attribution (CC BY) license (<http://creativecommons.org/licenses/by/4.0/>). <https://doi.org/10.1116/1.4996952>

I. INTRODUCTION

Hydrogel materials are increasingly used in important fields spanning from tissue engineering,¹ drug delivery,² implants,³ and wound dressings^{4,5} to various analytical technologies.^{6–8} Sensor and biosensor analytical applications typically take advantage of hydrogels that exhibit large surface area, are resistant to fouling by biomolecules present in complex media and can be tailored to provide additional biological function.^{9,10} They can be used as thin layers attached to a sensor surface that serves as a highly open binding matrix when postmodified with ligands specific to target analytes.^{11–13} Besides affinity biosensors for *in situ* detection of analyte species, hydrogels are also pursued to advance implanted biosensors by preventing adhesion of cells and thus prolong their lifetime.¹⁴ In addition, cell-on-chip microfluidic systems increasingly employ hydrogels that mimic the extracellular matrix, which allow for the design of complex

artificial architectures resembling 3D living tissues.^{15,16} Structuring of hydrogels was demonstrated to be key for culturing of specific cell types, for example, vascularization by endothelial cells,¹⁷ or neural cell network formation.¹⁸ More complex hydrogel microstructures have been exploited in microfluidic actuators for stimuli-responsive control of liquid flow,^{19–21} allowing fabrication of microfluidic valves^{22,23} and reservoirs for preconcentration of selected biomolecules.^{24,25}

Among the various geometries, hydrogel membranes attract increasing attention for many applications.²⁶ A variety of hydrogel membrane preparation techniques were reported. For instance, very thin (30–100 nm thick) membranes were prepared by layer-by-layer polymer deposition onto a sacrificial layer through spin-coating to form a suspended structure spanning over 10 μm gaps.²⁷ However, the majority of the free-standing hydrogel membranes reported are much thicker. A porous, flexible free-standing composite hydrogel film with around 7 μm thickness was fabricated by filtration of graphene and polyaniline hydrogel composite

^{a)}Electronic mail: jakub.dostalek@ait.ac.at

aggregates.²⁸ A crosslinked free-standing polyvinyl alcohol-based hydrogel film with 300 μm thickness was fabricated through solution casting in a predefined mold.²⁹ Free-standing hydrogel macrostructures are also reported for syringe polymerization to yield tubular or cylindrical hydrogel structures³⁰ or for molecular self-assembly into various predefined shapes.³¹ Free-standing structures with various shapes and functionalities make an attractive means for sensing applications. In a recent report, free-standing molecularly imprinted photonic hydrogels with thickness of around 100 μm were constructed through a colloidal crystal templating method and applied for the detection of analytes.³² A free-standing composite film composed of a gold nanoshell microsphere colloidal crystal and a polyacrylic acid-based hydrogel was prepared by photopolymerization and was utilized for sensing of pH changes.³³ Thermoresponsive poly(*N*-isopropyl) acrylamide (pNIPAAm) based free-standing hydrogel films (100–300 μm thickness) were constructed by injection compression molding, that could potentially be employed for cell-on-chip applications.³⁴ Free-standing polyethylene glycol diacrylate-based hydrogel films with a thickness around 200 μm were prepared by polymerizing between Teflon-coated quartz plates and with these high water intake, antifouling, antimicrobial, and oil/water filtration activities were demonstrated.³⁵ Recent studies have sought to improve hydrogel mechanical stability, stretchability,³⁶ and macroshaping³⁷ that could be further applied for wearable sensors or tissue engineering.

We report on the facile preparation of a mechanically robust, thermoresponsive, free-standing pNIPAAm hydrogel-polystyrene nanoparticle (PS NP) composite membranes that span over a distance of 100 μm across microfluidic channels with a mere film thickness as low as 1 μm . These free-standing hydrogel membranes are prepared by template stripping over a channel array casted onto a surface plasmon resonance (SPR) sensor chip. Rapid diffusion of low molecular weight molecules and soluble constituents present in blood plasma is investigated for these pNIPAAm-PS NP composite membranes, and their on demand switching from a permeable to a closed state is demonstrated by combined optical waveguide spectroscopy (OWS) and SPR measurements.

II. EXPERIMENT

A. Materials

D-(+)-maltose monohydrate was obtained from Carl Roth (Germany), phosphate buffered saline (PBS, 140 mM NaCl, 10 mM phosphate, 3 mM KCl, pH 7.4) was purchased from Calbiochem (Germany), off-stoichiometry thiol-ene polymer (OSTEmer 322 Crystal clear) was obtained from Mercene Labs (Sweden), Hellmanex III was obtained from Hellma Analytics, Polybead 100 nm microbeads (PS) were purchased from PolySciences (Germany), newborn calf serum was purchased from Invitrogen (Germany), and polydimethylsiloxane (PDMS, Sylgard 184) was obtained from Dow Corning.

B. Experimental setup and methodology

1. pNIPAAm-based polymer

The pNIPAAm-based terpolymer with 94:5:1 molar ratio of *N*-isopropylacrylamide, methacrylic acid, and 4-methacryloyloxy benzophenone was synthesized as previously described¹² and its structure is shown in Fig. 1(a).

2. 3,3'-disulfanediybis(*N*-(4-benzoylbenzyl)propanamide

For the surface attachment of the respective pNIPAAm-based composite films to the gold substrates, a novel benzophenone derivative with a disulfide anchor group was developed [see Fig. 1(b)]. For this purpose, bis(2,5-dioxopyrrolidin-1-yl)3,3'-disulfanediyldipropionate was reacted with 4-(aminomethyl)benzophenone (4-AMBP)³⁸ in the presence of triethylamine at room temperature (see Fig. S1).⁵² Bis(2,5-dioxopyrrolidin-1-yl)3,3'-disulfanediyldipropionate (0.74 mmol, 0.30 g) was dissolved in dimethyl sulfoxide (DMSO) (14 ml) and cooled with an ice-water bath to 0 °C. 4-(aminomethyl)benzophenone (3.30 mmol, 0.70 g) dissolved in DMSO (6 ml) and Et₃N (3.20 mmol, 0.45 ml) were added and the solution stirred for 16 h at room temperature. Dichloromethane (DCM) (20 ml) was added and the organic layer was washed with water (2 × 20 ml). The formed precipitate in the organic layer was filtered off and washed with small portions of DCM, followed by drying of the remaining product under reduced pressure. The yield was of 51% (0.38 mmol, 0.26 g) of a white solid. The resulting product was characterized by ¹H and ¹³C NMR spectroscopy (provided in the supplementary material, Figs. S2 and S3), showing only minor impurities of a monosubstituted product. IR spectroscopy showed bands (cm⁻¹) at 3295 (N-H), 3052 (C-H_{aromatic}), 2907 (C-H), and 1641 (C=O).

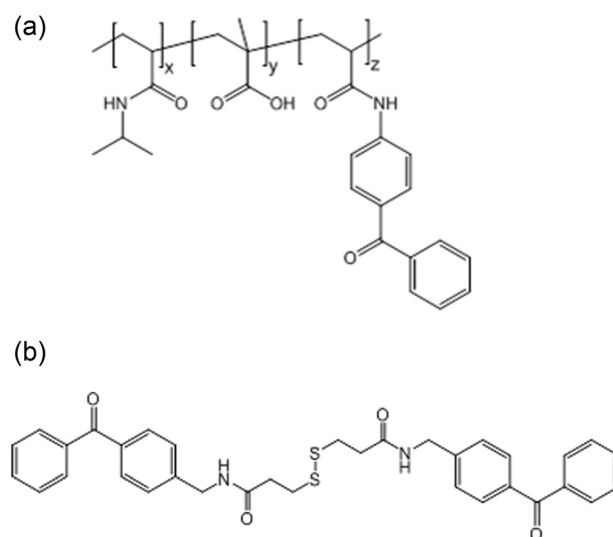


FIG. 1. Chemical structure of (a) the benzophenone-modified, crosslinkable, carboxylated pNIPAAm terpolymer and (b) the benzophenone-modified disulfide (4-AMBP-disulfide).

TABLE I. Prepared solutions of hydrogel-particle composites at various weight fraction ratios (r_c) of pNIPAAm and PS NP.

pNIPAAm (wt. %)	PS nanoparticles (wt. %)	Ratio PS/pNIPAAm, r_c
2.5	0	0
2.5	0.625	0.25
2.5	1.25	0.5
2.5	2.5	1
2.5	3.5	1.4
1	5	5

3. Nanocomposite hydrogel thin film preparation

Composite hydrogel films were prepared by spin-coating an ethanolic solution with dissolved pNIPAAm and suspended polystyrene nanoparticles at weight fractions as specified in Table I. These films were either attached directly to a gold surface for the SPR/OVS studies or on top of an array of OSTEmers channels in order to serve as a free-standing membrane. Both types of structures were prepared on BK7 glass substrates that were cut into 20×25 mm pieces and sequentially washed with 1% Hellmanex III solution, distilled

water, and absolute ethanol, amid sonicating, and dried under air stream. Subsequently, 2 nm chromium film and 50 nm thick gold films were deposited by vacuum thermal evaporation (HHV Auto306 Lab Coater).

For the preparation of attached composite films, gold-coated substrates were immersed overnight into 1 mM solution of 4-AMBP-disulfide dissolved in DMSO in order to form a self-assembled monolayer (SAM). Such benzophenone SAM-functionalized substrates were rinsed with copious amounts of ethanol and dried in a stream of air. An ethanolic solution with pNIPAAm and PS nanoparticles was then spun onto the sensor chip at 2000 rpm for 60 s followed by drying overnight at 50°C under vacuum (Heraeus Vacuum Oven VT 6025, Thermo Scientific). The resulting films were crosslinked and simultaneously attached to the sensor chip via the photoreactive 4-AMBP-disulfide SAM by exposure to 365 nm UV light with an irradiation dose of 4 J/cm^2 followed by rinsing with ethanol and dried before measurements.

In order to prepare a free-standing pNIPAAm/PS NP-based membrane, the modified procedure introduced in Fig. 2

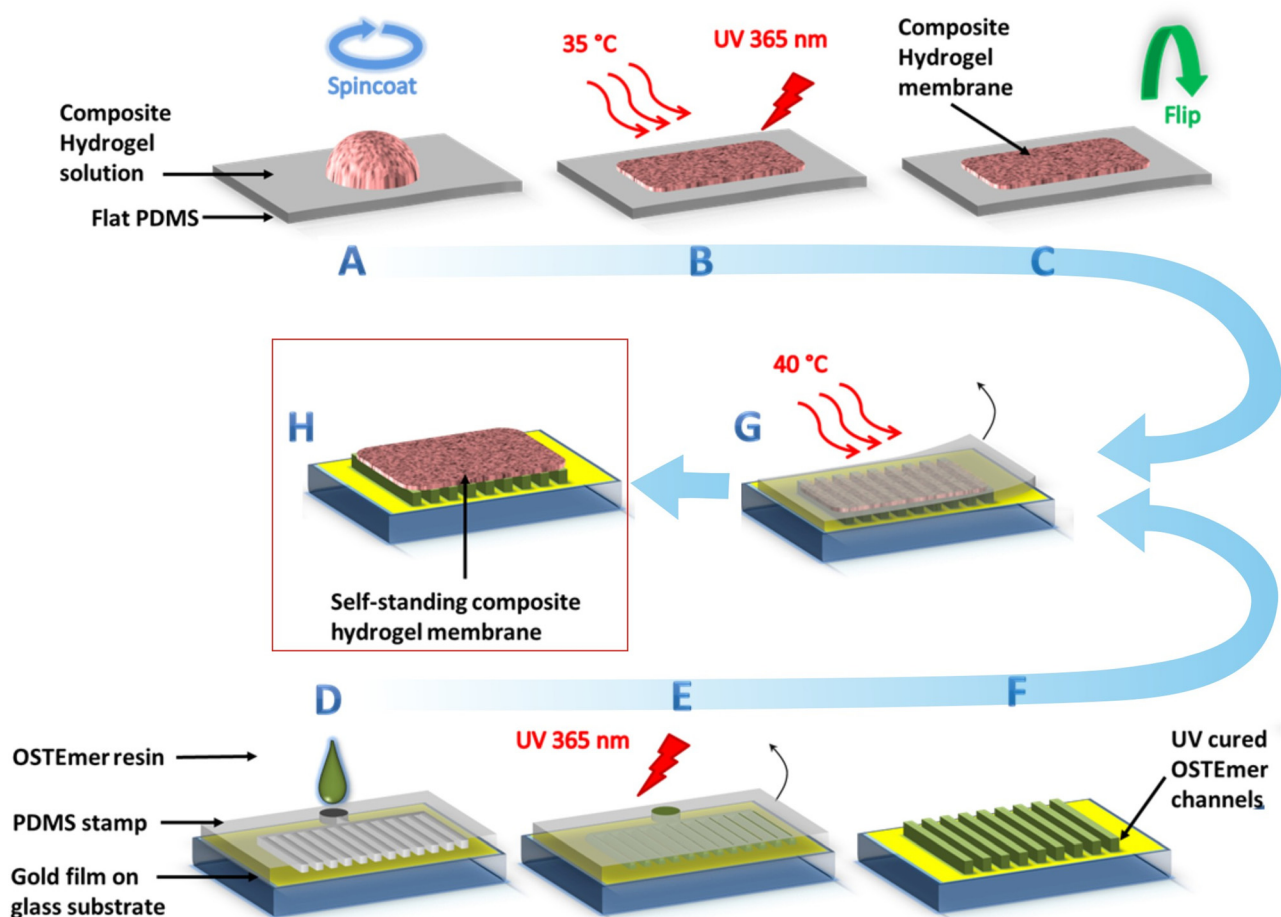


FIG. 2. Preparation of thin hydrogel composite films attached as a free-standing membrane spanning over narrow channels: (a) spin-coating, (b) drying and crosslinking hydrogel-PS NP composite film on flat PDMS (c). Meanwhile, (d) filling of PDMS channels with OSTEmers on gold surface followed by (e) UV curing and (f) detachment of the PDMS support to reveal epoxy-activated OSTEmers channel structures and subsequently (g) thermal hardening and bonding of OSTEmers channels to the composite hydrogel films. Finally, (h) lifting off the PDMS support to reveal dry, free-standing composite hydrogel membrane over OSTEmers channel structures.

was developed. First, the nanocomposite polymer layer was deposited (step A in Fig. 2) on a flat PDMS block ($2 \times 2 \times 0.5$ cm) by spin coating at 1000 rpm for 60 s followed by drying overnight at 35°C (step B in Fig. 2). Meanwhile, a PDMS stamp with casted arrays of grooves was placed above a gold-coated substrate (step D in Fig. 2) and the formed channels were filled with an OSTEmer resin by the capillary effect (step E in Fig. 2). The OSTEmer was then UV-cured with an irradiation dose of 0.8 J/cm^2 at a wavelength of 365 nm. Subsequently, the PDMS stamp was removed exposing arrays of adhesive OSTEmer ribs with reactive epoxy groups (step F in Fig. 2). The spin-coated, dried, and cross-linked pNIPAAm-based nanocomposite membrane on the flat PDMS (steps A–C in Fig. 2) was then placed over the OSTEmer structure and allowed to bond at 40°C overnight (step G in Fig. 2). Finally, the flat PDMS support was lifted off the polymer membrane to reveal a dry free-standing membrane spanning over the OSTEmer channel structure (step H in Fig. 2). The resulting cavities, which were capped with the composite pNIPAAm-based polymer films, had a depth of $d_c = 45\ \mu\text{m}$ and a width of $w_c = 30\text{--}95\ \mu\text{m}$.

4. Visualization of the hydrogel composite morphology

Hydrogel composite films and membranes were investigated using an optical microscope (Olympus BX51M) and a scanning electron microscope (SEM) operated at a low voltage of 5 kV (Carl Zeiss EVO). A 13 nm thick layer of platinum was sputtered (Cressington Sputter Coater 108auto) on the hydrogel composite films or membranes for SEM imaging.

5. Optical setup for SPR/OWS measurements

SPR and OWS measurements were carried out by using an optical setup with the Kretschmann configuration of attenuated total reflection which was described in our previous works in more detail.³⁹ As Fig. 3 shows, the glass substrate with hydrogel nanocomposite film was optically matched onto a LASFN9 glass prism with an appropriate immersion oil. A laser beam at $\lambda = 633\ \text{nm}$ was coupled to the prism to hit the gold surface at an angle θ . The angular reflectivity spectrum $R(\theta)$ was measured by using a rotation stage for transverse magnetic (TM) and transverse electric (TE) polarization. In order to flow aqueous samples over the surface of the pNIPAAm-based composite film, a flow cell was clamped and connected to a peristaltic pump (Ismatec, IDEX Health & Science SA, Switzerland) by using Tygon tubing with an inner diameter of $0.25\ \mu\text{m}$. For temperature-controlled permeability measurements, a Peltier element was integrated into a flow-cell as described before.¹¹ The probed area with the channels is completely contained within the flow-cell, and the channels were dead end in order to assure their sealing during flow experiments.

6. Acquisition and evaluation of SPR/OWS data

The swelling properties of hydrogel composite film attached to a gold surface were investigated by OWS. In this method, the refractive index n_h and thickness d_h of the layer as well as the refractive index of the bulk solution n_s were determined by fitting the measured angular reflectivity spectra $R(\theta)$. These spectra exhibit series of characteristic dips due to the resonant excitation of surface plasmons (SPs) and higher waveguide modes ($\text{TEM}_{1,2,\dots}$). As can be seen in Fig. S3 in the supplementary material, the resonance coupling to waveguide

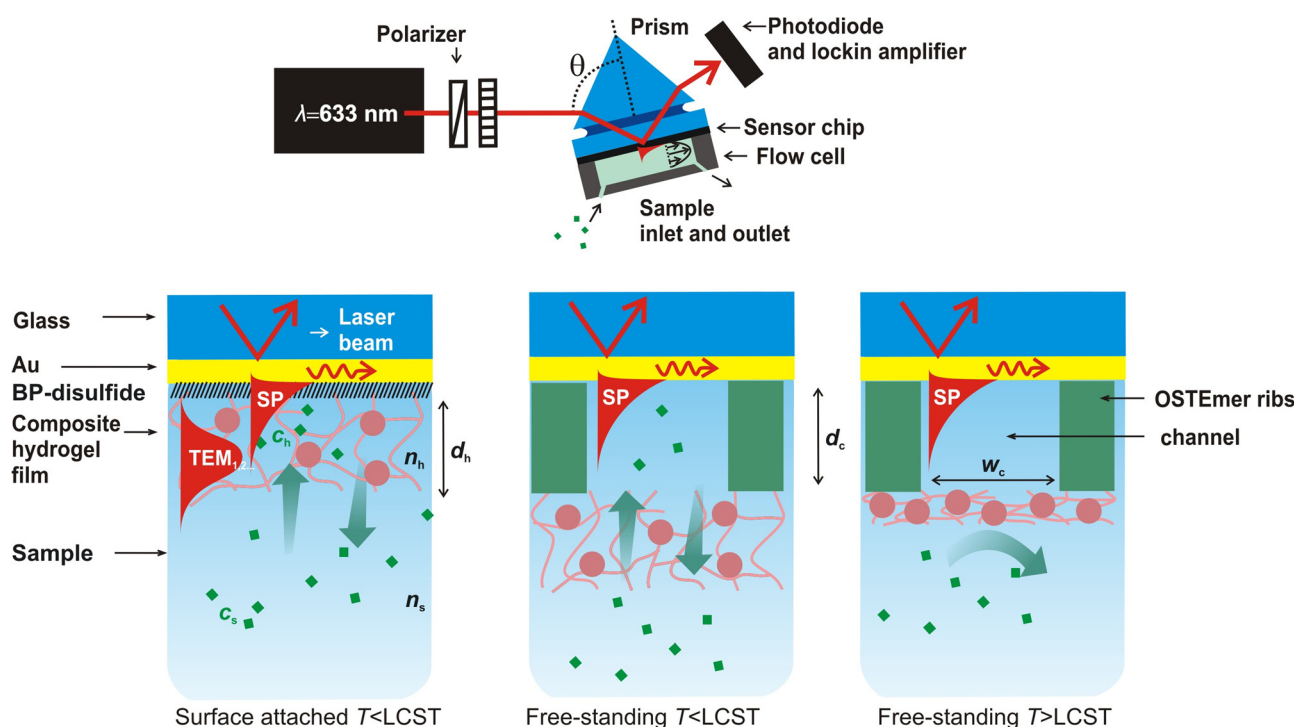


FIG. 3. Optical setup for the observation of thin hydrogel films and diffusion of biomolecules based on combined SPR and OWS.

modes TM_1 and TE_0 manifests itself as respective dips with the minima centered at distinct angles θ_{TM} and θ_{TE} . In addition, one can see an abrupt change in the reflectivity occurring at a critical angle θ_c . By using transfer matrix-based model implemented in the software Winspall (MPI for Polymer Research, Germany), three parameters were determined by fitting three angles θ_{TM} , θ_{TE} , and θ_c refractive index n_h and thickness d_h of the prepared composite films and the refractive index of the bulk solution n_s .⁴⁰ The parameters of other materials including the BK7 glass substrate, chromium, gold and disulfide linker SAM layers were kept constant throughout all fitting as determined by reference measurements on substrates without the composite.

For the study of permeation of blood serum and low molecular weight maltose analyte to the attached composite hydrogel film, changes in the refractive index of the film n_h were compared to those measured for the solution n_s flowed over the surface. The changes in these refractive indices Δn_s and Δn_h were assumed to be proportional to the concentration of the analyte molecules in the liquid sample c_s and in the hydrogel composite c_h , respectively. Consequently, the concentration ratio of biomolecules in the layer and that in the sample relates directly to the corresponding ratio of refractive index changes $c_h/c_s = \Delta n_h/\Delta n_s$. Such dependence can be obtained from the Maxwell-Garnett effective medium theory for small refractive index changes $\Delta n_h \ll n_h$ and $\Delta n_s \ll n_s$. It is worth noting that from the hydrogel thickness d_h and refractive index n_h its surface mass density can be obtained as $\Gamma = (n_h - n_s) \times d_h \times \partial n/\partial c$, where $\partial n/\partial c = 0.2 \mu\text{l}/\text{mg}$ for the majority of organic materials such as proteins and synthetic polymers. In order to observe the unspecific sorption of biomolecules into the composite hydrogel network, the change in the surface mass density $\Delta\Gamma$ can be measured before and after the contact of analyzed sample with the composite film. The accuracy with which the surface mass density change $\Delta\Gamma$ due to the deposit in the composite hydrogel film is determined is limited by the precision with which the resonant angles θ_{TM} , θ_{TE} , and θ_c are measured. The used rotation stage with increments of 0.01° allowed to resolve surface mass density changes down to $\sim 1 \text{ ng}/\text{mm}^2$.

For the study of permeation of low molecular weight analyte through the free-standing hydrogel composite membrane, the gold surface at the bottom of the OSTEmer channel was probed by resonantly excited SPs (see bottom right of Fig. 3). Changes in the reflectivity R due to the bulk refractive index changes induced by the analyte diffusion through the hydrogel membrane to underneath cavity were recorded in time at incidence angle θ fixed at the slope of the SPR dip. It is worth to note that the penetration depth of resonantly excited SPs of about 100 nm is much shorter than the height of the cavity $d_c = 45 \mu\text{m}$ and thus the measured SPR changes are not affected by the membrane itself and the upper medium.

III. RESULTS AND DISCUSSION

In order to prepare free standing hydrogel membrane and to demonstrate their switching between permeable and

closed states, the following experiments were carried out. First, the preparation of composite films was optimized and their key characteristics were determined. The preparation of free-standing membranes was observed by the use of microscopy and their thickness, density, and permeability was observed by OWS when attached to a substrate. These properties were measured as a function of loading PS nanoparticles to the hydrogel material in order to reinforce the membrane by reducing its swelling. Lastly, the free-standing responsive hydrogel composite membrane prepared through the established protocol was tested for dynamically controlled permeability triggered by external stimulus.

A. Morphology of prepared membranes

The surface morphology of the crosslinked polymer films being composed of pNIPAAm-based polymer and PS nanoparticles was first scrutinized by SEM. The panels of the left row in Fig. 4 show the acquired top view for films prepared with the weight fraction ratio for PS nanoparticles versus pNIPAAm of $r_c = 0.25, 0.5, \text{ and } 1$. These images reveal that the PS nanoparticles are homogeneously embedded in the pNIPAAm matrix and that an increasing concentration of the nanoparticles in the solution spun on the surface leads to an apparent increase of the NP density in the film. For the studied range, the middle and right panels of Fig. 4 confirm that the dry composite films with a thickness of $d_{h\text{-dry}} = 70\text{--}280 \text{ nm}$ could be successfully transferred on top of the OSTEmer channels with a width of $w_c = 30 \mu\text{m}$. From previous studies of the pNIPAAm matrix on planar PS substrates, it can be inferred that the PS particles are covalently attached to the pNIPAAm network after photocrosslinking,⁴¹ which is also corroborated by the robustness of the composite membrane in the swelling studies described below.

B. Swelling properties of nanocomposite films

When exposed to aqueous media, the hydrogel matrix is able to swell and form a permeable structure. To test the swelling of prepared membranes spanning over the channels in water, optical microscopy was used. Figure 5 shows a series of images obtained for hydrogel films with varied composition $r_c = 0, 0.25, 0.5, \text{ and } 1$. The upper panel was measured in water at room temperature $T = 20^\circ\text{C}$, and the lower panel was measured after removing the water and letting the membrane dry for 10 min at room temperature. The composite hydrogel membranes show 3D swelling behavior that leads to their buckling. However, with increasing content of PS particles, the composite hydrogel membranes swell less, which reduces this effect. The increasing mechanical rigidity of the hydrogel composite membrane was visually observed during preparation; however, membranes with the higher concentrations of PS ($r_c = 0.5$ and 1) were more brittle.

With the aim of characterizing the role of embedded PS nanoparticles on the swelling behavior of hydrogel membranes, OWS was used to measure the changes in the swelling ratio (SR) of the composite films attached to a planar

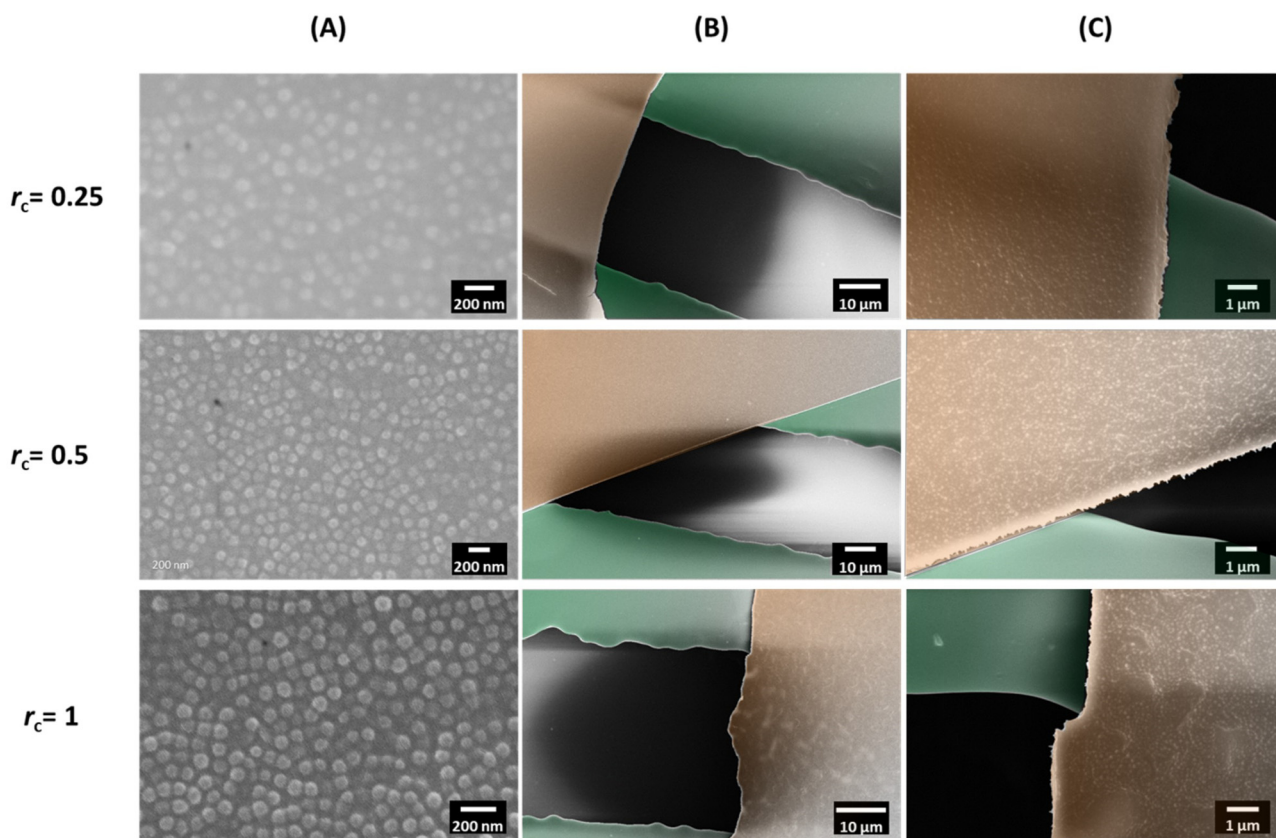


FIG. 4. SEM images of dry prepared composite films. Columns show (a) top view of composite films, (b) broad view of a free-standing composite membrane (false red color) spanning over a channel formed by OSTemer (false green color) and (c) close-up view of the edge of the free-standing composite membrane.

gold surface. The SR of composite films was calculated as the ratio of the swollen film thickness d_h to the dry thickness $d_{h\text{-dry}}$. The measured dependence on the loading with PS nanoparticles r_c is presented in Fig. 6. The SR of hydrogel composite is strongly suppressed by a factor of about twofold

when PS nanoparticle loading is $r_c = 0.25$ compared to the native hydrogel film ($r_c = 0$). Further reduction in the swelling of hydrogel composite films with increased loading of PS nanoparticles is observed. For higher PS loads of $r_c = 1$ and 5, almost no swelling occurs, as evidenced by the measured

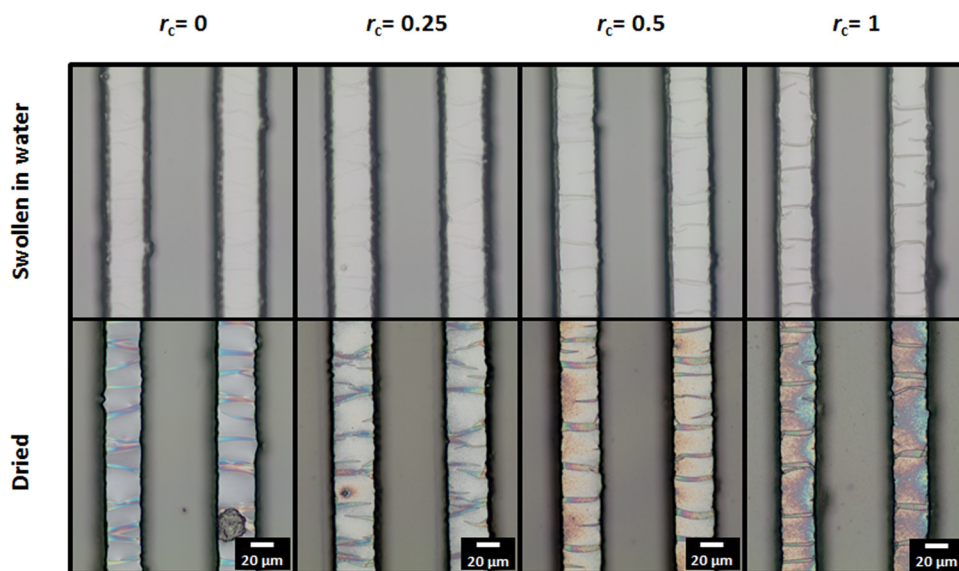


FIG. 5. Optical microscope images of free-standing composite membranes spanning over a 30 μm -wide microfluidic channel. Columns show structures with varied wt. % PS/pNIPAAm ratio $r_c = 0, 0.25, 0.5$, and 1. Upper row shows images acquired in water and bottom row after drying in air.

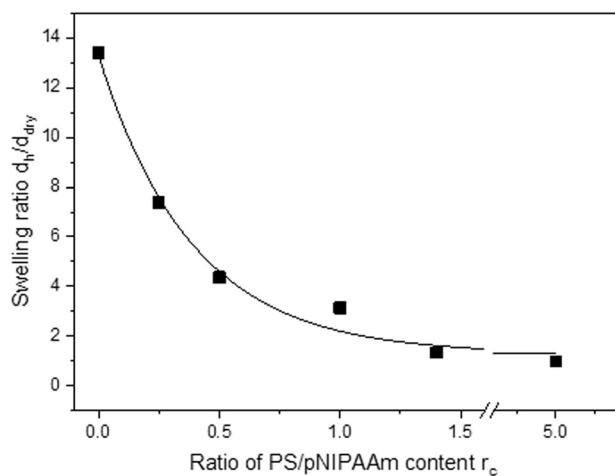


FIG. 6. Swelling ratio of surface-attached hydrogel composite films with varying loading ratio of PS nanoparticles in the pNIPAAm matrix. Temperature of measurement $T = 20^\circ\text{C}$.

SR of around 1. The reduction or the SR for composite hydrogels with PS nanoparticles is consistent with previous reports of a similar system.⁴²

The SR relates to the mesh size of the polymer networks. For instance, for a similar native pNIPAAm hydrogel film swollen in ethanol with $\text{SR} = 12$ exhibited a mesh size of 3.4 nm as determined by fluorescence correlation spectroscopy.⁴³ In addition, it is worth noting that the herein performed OWS measurements capture only swelling in the direction perpendicular to the substrate plane as the studied films were covalently attached to the solid substrate. In contrast, the swelling of free-standing membranes can also occur laterally by a buckling mode (visible in Fig. 5), which the OWS data does not take into account.

C. Permeability of the attached nanocomposite films

For the observation of diffusion of biomolecules through the composite membrane, the same OWS technique was employed with a series of aqueous sample being flowed over the surface-attached composite films. The diffusion of biomolecules dissolved in such liquid samples was determined from the measured refractive index changes Δn_s and Δn_c which are directly proportional to the biomolecule concentration. These measurements were performed at $T = 20^\circ\text{C}$, which is below the lower critical solution temperature (LCST) of the pNIPAAm matrix in order to assure appropriate swelling.

First, diffusion of the small analyte maltose with a molecular weight of 0.36 kDa, dissolved in PBS buffer at a concentration of $c_s = 0.2\text{ M}$, was measured. Before the beginning of the diffusion experiments, each composite film was exposed to PBS solution to allow equilibrium swelling. Then, PBS with maltose was flowed for more than 10 min until equilibrium in diffusion was reached. The reflectivity spectra were measured for the structures immersed in PBS and in PBS with maltose (see Fig. S3 in the supplementary material). The analysis of the acquired spectra allowed the determination of the maltose concentration in the composite film that

was normalized with that in the bulk solution c_h/c_s . Results in Fig. 7 show a slow decrease of the c_h/c_s from about 0.85 to 0.4 when increasing the loading of PS nanoparticles in the composite from $r_c = 0$ to 5. These data indicate efficient diffusion of the low molecular weight analyte through the hydrogel network between the PS nanoparticles (which are impermeable by the aqueous solution) and are consistent with complementary fluorescence correlation spectroscopy data on diffusion of small fluorophore tracers.⁴⁴

In order to assess information on the diffusion of biomolecules with larger molecular weight, the interaction of composite films with undiluted blood serum was studied by OWS. The majority of proteins present in serum exhibit a molecular weight between 66 and 160 kDa and hydrodynamic radii (3.4 and 6.5 nm, respectively) which is comparable or above the estimated mesh size of the hydrogel (3–5 nm according to fluorescence correlation spectroscopy^{44,45}). The obtained data presented in Fig. 7 indicate that for a hydrogel film without PS nanoparticles, the concentration of biomolecules that diffuse into the polymer network is ten times lower compared to that in serum $c_h/c_s = 0.1$. When decreasing the SR by introducing PS nanoparticles, the permeation of proteins is further hindered to $c_h/c_s = 0.03$ for $r_c = 1.5$. Surprisingly, the amount of serum proteins that is present in the composite film is enhanced to about $c_h/c_s = 0.25$ when increasing the loading with PS nanoparticles to $r_c = 5$. This effect can be attributed to only partial coverage of PS nanoparticles with pNIPAAm hydrogel which leads to unspecific sorption of proteins to polystyrene surface. In addition, the mechanical swelling stress may lead to the occurrence of cracks of brittle membranes with high r_c . This effect in conjunction with low content of hydrogel can strongly increase the pore size to values much greater than the hydrodynamic radius of large proteins like IgG ($R_h = 6.5\text{ nm}$).⁴⁵ It is worth noting that a similar effect

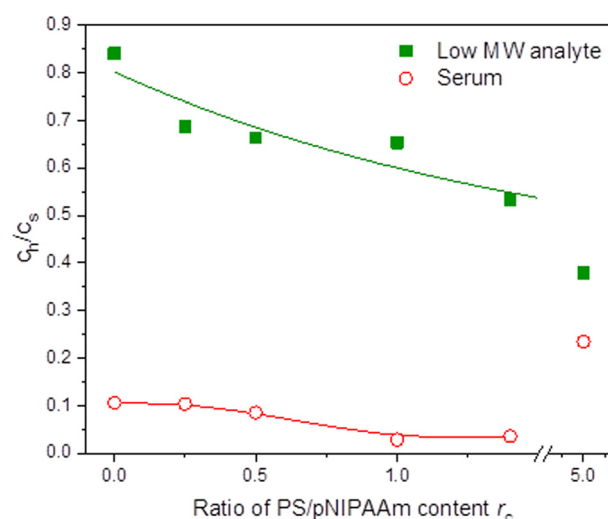


FIG. 7. OWS investigation of the diffusion of a low molecular weight analyte (maltose, $\text{MW} = 0.36\text{ kD}$, at a concentration of 0.2 M in PBS buffer) and undiluted blood serum (molecular weights of major protein components 66–160 kDa) through the surface-attached hydrogel composite film with varying wt. % ratio of PS NP/pNIPAAm $r_c = 0$ –5.

was observed for the pNIPAAm-based composite film with molecularly imprinted polymer nanoparticles.⁴⁶

In order to distinguish between protein molecules diffusion through the membrane and their unspecific sorption, OWS measurements were performed after the exposure to undiluted serum for 30 min and rinsing with PBS for 10 min. Indeed, the fouling effect of the network with serum was not measurable for the composites with $r_c = 0$ –1.5. Contrary to these results, composite with very high nanoparticle content $r_c = 5$ showed a significant increase in the refractive index $\Delta n_h = 2 \times 10^{-4}$ due to the unspecific sorption of serum proteins. This value translates to an increase in the surface mass density of the composite film by 2.1% and it can be attributed to the fact that at high r_c , PS nanoparticles are not capped with hydrophilic pNIPAAm hydrogel and thus are prone to unspecific sorption of proteins.^{46,47}

D. Permeability of free-standing nanocomposite film

The permeability of the free-standing membrane spanning the channel structure (refer to scheme in Fig. 2), which was prepared with a thickness of $\sim 1 \mu\text{m}$ and PS nanoparticles loading of $r_c = 0.33$, was tested for the low molecular weight analyte maltose. In these experiments, the possibility to reversibly switch the permeation by controlling the swelling state of the pNIPAAm-based membrane with temperature was explored. The pNIPAAm polymer exhibits a lower critical solution temperature at $\text{LCST} = 32^\circ\text{C}$ and increasing the temperature above the LCST leads to the collapse of the networks. In the collapsed state, a denser membrane will result possessing a smaller pore size. The transport of maltose through the composite film in the permeable “open” state at $T = 20^\circ\text{C}$ and in the collapsed “closed” state at $T = 40^\circ\text{C}$ was monitored by probing the liquid volume in the channel below the membrane by resonantly excited SPs at the gold surface (see Fig. 3). The distance of the membrane from the gold was of about $d_c = 45 \mu\text{m}$ which is more than 2 orders of magnitude longer than the probing depth of the evanescent SP field of about $0.1 \mu\text{m}$. Therefore, the measured changes in SPR can be specifically attributed to only species that diffuse into the cavity through the membrane.

First, the membrane was heated to $T = 40^\circ\text{C}$ (collapsed state) and water was circulated through the flow-cell over the top of the composite membrane. After equilibration to establish a stable baseline in the SPR signal, the 0.2 M maltose PBS solution at this elevated temperature was injected at $t = 5 \text{ min}$ followed by rinsing with warm water at $t = 12 \text{ min}$. The respective SPR kinetics are shown in Fig. 8 (curve 1). Apparently, the maltose diffusion across the membrane is hindered at $T = 40^\circ\text{C}$; thus, no measurable increase in the refractive index within the channel under the membrane occurs.

Second, the membrane was cooled to $T = 20^\circ\text{C}$ and the same experiment was repeated. Contrary to the previous data, the measured curve 2 in Fig. 8 shows that the injection of maltose induces a strong increase in the SPR signal after $t = 5 \text{ min}$, which reaches equilibrium after several minutes.

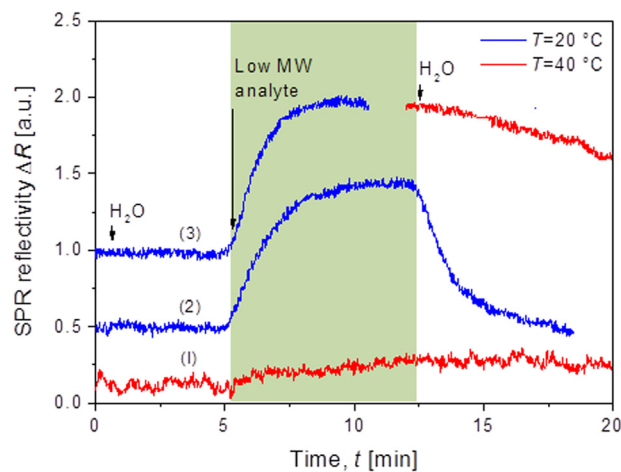


FIG. 8. SPR investigation of diffusion of low molecular weight analyte (maltose, MW = 0.36 kD, dissolved 0.5 mM in PBS buffer) across the free-standing PS/pNIPAAm composite membrane with $r_c = 0.25$. The permeability of the membrane was switched by changing the temperature from the open state at $T = 20^\circ\text{C}$ below the LCST of NIPAAm (around 32°C) to the closed state at $T = 40^\circ\text{C}$ above the LCST. Curves (1) indicate the closed state, (2) the open state, and (3) diffusion of molecules through open membrane and their trapping by switching to the closed state.

When rinsing the top flow cell with cold water, the maltose quickly diffuses out through the membrane, which is manifested as a decrease in the reflectivity after $t = 12 \text{ min}$. The observed time response of several minutes is in agreement with the diffusion-controlled transfer, which can be described based on Fick’s law as $\Delta t \sim d_c^2/D$. Assuming a diffusion coefficient of maltose of $D = 5 \times 10^{-6} \text{ cm}^2 \text{ s}^{-1}$,⁴⁸ the characteristic time of $\Delta t \sim 5 \text{ s}$ is predicted to fill the channels. The measured response time in the minute range is significantly longer, which can be ascribed to the slower, hindered diffusion through the hydrogel composite membrane and to the mixing occurring upon the transport in the flow-cell and tubing.

Finally, the membrane was kept at $T = 20^\circ\text{C}$ for which maltose can diffuse through the swollen composite membrane and fill the probed channels. After saturating the liquid volume in the channel with maltose, the membrane was heated to $T = 40^\circ\text{C}$ which switches it to the collapsed, non-permeable state. As curve 3 in Fig. 8 reveals, when the volume of the flow-cell above was rinsed with warm water, the diffusion of maltose through the sealed membrane is strongly hindered and only a slow decrease in the SPR signal is observed.

IV. SUMMARY AND CONCLUSIONS

In this report, PS nanoparticles were incorporated into a pNIPAAm hydrogel matrix to produce free-standing hydrogel membranes with improved mechanical stability. We utilized a thiol-ene-epoxy resin OSTEmmer to fabricate microchannel structures that can be firmly bound to the hydrogel composite in a simple two-step process, yielding a free-standing membrane over a total area of about one square millimeter. The investigation of the morphology in the hydrogel-nanoparticle

composite revealed a reduced bulging of the membranes when swollen in water as compared to a neat hydrogel membrane without PS nanoparticles. Surface-attached films of these hydrogel composites were investigated by SPR/OWS for their swelling behavior, as well as the selective permeability for low molecular-weight compound and large proteins present in complex blood serum samples. Hydrogel composites with an excess of the hydrogel component compared to the PS nanoparticle content showed efficient semipermeability to maltose while blocking serum proteins, as well as sound nonfouling capability. In contrast, an excess of PS nanoparticle loading in the hydrogel matrix leads to an enhanced adsorption of the serum proteins (potentially by a large increase of the fouling PS particle surface), in addition to loss of the semipermeability. Finally, the thermal response of the swelling state in the pNIPAAm hydrogel was exploited to dynamically control the permeability of the free-standing composite membrane. The SPR observation showed rapid diffusion of low molecular weight molecules through the swollen membrane at temperatures below the LCST of 32 °C and blocking of the diffusion when collapsing the hydrogel at a temperature well above its LCST. The herein reported semipermeable, free-standing hydrogel composite membranes can be applied to various microstructures and microfluidic architectures, paving the way for a wide range of novel applications in lab-on-a-chip⁴⁹ or biosensing⁵⁰ of crude samples (e.g., whole blood or serum).⁵¹

ACKNOWLEDGMENTS

K.S. acknowledges financial support from the Austrian Federal Ministry for Transport, Innovation and Technology (GZ BMVIT-612.166/0001-III/II/2010). C.P. was partially supported by the European Union's Horizon 2020 research and the innovation program under Grant Agreement No. 633937, project ULTRAPLACAD.

- ¹F. Chen *et al.*, *Sci. Rep.* **6**, 20014 (2016).
- ²T. Billiet, M. Vandenhoute, J. Schelfhout, S. Van Vlierberghe, and P. Dubruel, *Biomaterials* **33**, 6020 (2012).
- ³A. K. Riau *et al.*, *ACS Biomater. Sci. Eng.* **1**, 1324 (2015).
- ⁴J. Li and D. J. Mooney, *Nat. Rev. Mater.* **1**, 16071 (2016).
- ⁵C. M. Magin, D. B. Neale, M. C. Drinker, B. J. Willenberg, S. T. Reddy, K. M. D. La Perle, G. S. Schultz, and A. B. Brennan, *Exp. Biol. Med.* **241**, 986 (2016).
- ⁶G. Sun *et al.*, *Proc. Natl. Acad. Sci. U. S. A.* **108**, 20976 (2011).
- ⁷D. Puchberger-Enengl, C. Krutzler, F. Keplinger, and M. J. Vellekoop, *Lab Chip* **14**, 378 (2014).
- ⁸H. Vaisocherova, W. Yang, Z. Zhang, Z. Q. Cao, G. Cheng, M. Piliarik, J. Homola, and S. Y. Jiang, *Anal. Chem.* **80**, 7894 (2008).
- ⁹A. Mateescu, Y. Wang, J. Dostalek, and U. Jonas, *Membranes* **2**, 40 (2012).
- ¹⁰T. Ekblad *et al.*, *Biomacromolecules* **9**, 2775 (2008).
- ¹¹A. Aulasevich, R. F. Roskamp, U. Jonas, B. Menges, J. Dostálek, and W. Knoll, *Macromol. Rapid Commun.* **30**, 872 (2009).
- ¹²Y. Wang, A. Brunsen, U. Jonas, J. Dostalek, and W. Knoll, *Anal. Chem.* **81**, 9625 (2009).
- ¹³O. Andersson, A. Larsson, T. Ekblad, and B. Liedberg, *Biomacromolecules* **10**, 142 (2009).
- ¹⁴R. M. Gant, A. A. Abraham, Y. Hou, B. M. Cummins, M. A. Grunlan, and G. L. Cote, *Acta Biomater.* **6**, 2903 (2010).
- ¹⁵X. J. Li, A. V. Valadez, P. Zuo, and Z. H. Nie, *Bioanalysis* **4**, 1509 (2012).
- ¹⁶M. B. Chen, S. Sriganapalan, A. R. Wheeler, and C. A. Simmons, *Lab Chip* **13**, 2591 (2013).
- ¹⁷S. Muehleider, A. Ovsianikov, J. Zipperle, H. Redl, and W. Holthöner, *Front. Bioengin. Biotechnol.* **2**, 52 (2014).
- ¹⁸K. Yoichi, N. Yoji, Y. Yuya, Y. Masumi, and S. Minoru, *Biofabrication* **6**, 035011 (2014).
- ¹⁹L. Dong and H. Jiang, *Soft Matter* **3**, 1223 (2007).
- ²⁰X. Zhang, L. Li, and C. Luo, *Lab Chip* **16**, 1757 (2016).
- ²¹D. H. Kang, S. M. Kim, B. Lee, H. Yoon, and K.-Y. Suh, *Analyst* **138**, 6230 (2013).
- ²²D. J. Beebe, J. S. Moore, J. M. Bauer, Q. Yu, R. H. Liu, C. Devadoss, and B.-H. Jo, *Nature* **404**, 588 (2000).
- ²³R. H. Liu, Y. Qing, and D. J. Beebe, *J. Microelectromech. Syst.* **11**, 45 (2002).
- ²⁴R. R. Niedl and C. Beta, *Lab Chip* **15**, 2452 (2015).
- ²⁵T. Shay, M. D. Dickey, and O. D. Velev, *Lab Chip* **17**, 710 (2017).
- ²⁶I. Tokarev and S. Minko, *Adv. Mater.* **21**, 241 (2009).
- ²⁷C. Jiang and V. V. Tsukruk, *Soft Matter* **1**, 334 (2005).
- ²⁸M. Moussa, Z. Zhao, M. F. El-Kady, H. Liu, A. Michelmore, N. Kawashima, P. Majewski, and J. Ma, *J. Mater. Chem. A* **3**, 15668 (2015).
- ²⁹N. Batisse and E. Raymundo-Piñero, *J. Power Sources* **348**, 168 (2017).
- ³⁰J. Sun, B. V. K. J. Schmidt, X. Wang, and M. Shalom, *ACS Appl. Mater. Interfaces* **9**, 2029 (2017).
- ³¹M. Lovrak, W. E. J. Hendriksen, C. Maity, S. Mytnyk, V. van Steijn, R. Eelkema, and J. H. van Esch, *Nat. Commun.* **8**, 15317 (2017).
- ³²Z. Yang, D. Shi, M. Chen, and S. Liu, *Anal. Methods* **7**, 8352 (2015).
- ³³D. D. Men *et al.*, *J. Mater. Res.* **32**, 717 (2017).
- ³⁴S. Tommaso, M. Federico, T. Alessandro, G. Federico, W. Patrick, M. Paolo, and L. Cristina, *J. Micromech. Microeng.* **22**, 105033 (2012).
- ³⁵Y.-H. La, B. D. McCloskey, R. Sooriyakumaran, A. Vora, B. Freeman, M. Nassar, J. Hedrick, A. Nelson, and R. Allen, *J. Membr. Sci.* **372**, 285 (2011).
- ³⁶J.-Y. Sun, X. Zhao, W. R. K. Illeperuma, O. Chaudhuri, K. H. Oh, D. J. Mooney, J. J. Vlassak, and Z. Suo, *Nature* **489**, 133 (2012).
- ³⁷Z. L. Wu, M. Moshe, J. Greener, H. Therien-Aubin, Z. Nie, E. Sharon, and E. Kumacheva, *Nat. Commun.* **4**, 1586 (2013).
- ³⁸R. F. Roskamp, "Functional hydrogels," Ph.D. thesis (Johannes Gutenberg-Universität, Mainz, 2009).
- ³⁹M. J. N. Junk, U. Jonas, and D. Hinderberger, *Small* **4**, 1485 (2008).
- ⁴⁰M. Toma, U. Jonas, A. Mateescu, W. Knoll, and J. Dostalek, *J. Phys. Chem. C* **117**, 11705 (2013).
- ⁴¹I. Anac, A. Aulasevich, M. J. N. Junk, P. Jakubowicz, R. F. Roskamp, B. Menges, U. Jonas, and W. Knoll, *Macromol. Chem. Phys.* **211**, 1018 (2010).
- ⁴²J. Dostálek and W. Knoll, *Polymer Science: A Comprehensive Reference*, edited by M. Möller (Elsevier, Amsterdam, 2012), pp. 647–659.
- ⁴³C. R. van den Brom, I. Anac, R. F. Roskamp, M. Retsch, U. Jonas, B. Menges, and J. A. Preece, *J. Mater. Chem.* **20**, 4827 (2010).
- ⁴⁴M. Gianneli, R. F. Roskamp, U. Jonas, B. Loppinet, G. Fytas, and W. Knoll, *Soft Matter* **4**, 1443 (2008).
- ⁴⁵R. Raccis, R. Roskamp, I. Hopp, B. Menges, K. Koynov, U. Jonas, W. Knoll, H. J. Butt, and G. Fytas, *Soft Matter* **7**, 7042 (2011).
- ⁴⁶N. Sharma *et al.*, *Macromol. Chem. Phys.* **215**, 2295 (2014).
- ⁴⁷*Product literature, Polymer Microspheres* (PolySciences, 2013), Vol. 2017, available at www.PolySciences.com.
- ⁴⁸H. Uedaira and H. Uedaira, *Bull. Chem. Soc. Jpn.* **42**, 2140 (1969).
- ⁴⁹M. Lundqvist, J. Stigler, G. Elia, I. Lynch, T. Cedervall, and K. A. Dawson, *Proc. Nat. Acad. Sci.* **105**, 14265 (2008).
- ⁵⁰D. Sticker, S. Lechner, C. Jungreuthmayer, J. Zanghellini, and P. Ertl, *Anal. Chem.* **89**, 2326 (2017).
- ⁵¹H. Im, N. J. Wittenberg, A. Lesuffleur, N. C. Lindquist, and S.-H. Oh, *Chem. Sci.* **1**, 688 (2010).

⁵²See supplementary material at <https://doi.org/10.1116/1.4996952> for synthesis, ¹H NMR and ¹³C NMR spectra of 3,3'-disulfanediybis(*N*-(4-benzoylbenzyl)propanamide), and angular reflectivity spectra of composite films.